

## Research Paper

# Multi-Scale Optical Imaging of the Delayed Type Hypersensitivity Reaction Attenuated by Rapamycin

Meijie Luo<sup>1,2</sup>, Zhihong Zhang<sup>1,2,✉</sup>, Hui Li<sup>1,2</sup>, Sha Qiao<sup>1,2</sup>, Zheng Liu<sup>1,2</sup>, Ling Fu<sup>1,2</sup>, Guanxin Shen<sup>3</sup> and Qingming Luo<sup>1,2,✉</sup>

1. Bitton Chance Center for Biomedical Photonics, Wuhan National Laboratory for Optoelectronics-Huazhong University of Science and Technology (WNLO-HUST), Wuhan 430074, China;
2. MoE Key Laboratory for Biomedical Photonics, Department of Biomedical Engineering, Huazhong University of Science and Technology (HUST), Wuhan 430074, China;
3. Department of Immunology, Tongji Medical College, Huazhong University of Science and Technology, Wuhan 430030, China.

✉ Corresponding author: E-mail: qluo@mail.hust.edu.cn or czyzzh@mail.hust.edu.cn.

© Ivyspring International Publisher. This is an open-access article distributed under the terms of the Creative Commons License (<http://creativecommons.org/licenses/by-nc-nd/3.0/>). Reproduction is permitted for personal, noncommercial use, provided that the article is in whole, unmodified, and properly cited.

Received: 2013.09.03; Accepted: 2013.12.07; Published: 2014.01.11

## Abstract

Neutrophils and monocytes/macrophages (MMs) play important roles in the development of cell-mediated delayed type hypersensitivity (DTH). However, the dynamics of neutrophils and MMs during the DTH reaction and how the immunosuppressant rapamycin modulates their behavior *in vivo* are rarely reported. Here, we take advantage of multi-scale optical imaging techniques and a footpad DTH reaction model to non-invasively investigate the dynamic behavior and properties of immune cells from the whole field of the footpad to the cellular level. During the classic elicitation phase of the DTH reaction, both neutrophils and MMs obviously accumulated at inflammatory foci at 24 h post-challenge. Rapamycin treatment resulted in advanced neutrophil recruitment and vascular hyperpermeability at an early stage (4 h), the reduced accumulation of neutrophils (> 50% inhibition ratio) at 48 h, and the delayed involvement of MMs in inflammatory foci. The motility parameters of immune cells in the rapamycin-treated reaction at 4 h post-challenge displayed similar mean velocities, arrest durations, mean displacements, and confinements as the classic DTH reaction at 24 h. These results indicate that rapamycin treatment shortened the initial preparation stage of the DTH reaction and attenuated its intensity, which may be due to the involvement of T helper type 2 cells or regulatory T cells.

Key words: Delayed type hypersensitivity, fluorescent imaging, motility, rapamycin, neutrophils, monocyte/macrophage.

## Introduction

Delayed type hypersensitivity (DTH), which is a cell-mediated immune response, is a double-edged sword that is required for host defense against etiologic agents but can also lead to pathologic responses and tissue damage. DTH is involved in antitumor immunity [1] and many types of clinical pathology, including graft rejection [2], mycobacterium tuberculosis infection [3], contact dermatitis [4], rheumatoid arthritis [5], and Crohn's disease [6]. DTH can occur in any tissue following an interaction of either T helper

type 1 (Th1) or T helper type 2 (Th2) cells with effector leukocytes. DTH consists of a sensitization phase followed by an elicitation phase, which is induced by antigen challenge in the sensitized individual and results in local inflammation. In addition to the key role of T cells, recent studies of different DTH models have shown that innate immune cells, including neutrophils and monocytes/macrophages (MMs), play important roles in the development of the DTH reaction.

Rapamycin is usually used as an immunosuppressant drug to prevent graft rejection in organ transplantation and in clinical therapy. In addition to its immunosuppressive effects on T lymphocytes, emerging studies show that rapamycin shapes the function of innate immune cells [7, 8]. Some studies have demonstrated that rapamycin can inhibit phagocytosis and chemotaxis of macrophages [9] and potently suppresses the polarity and chemotaxis of neutrophils [10, 11]. However, the regulatory mechanism of rapamycin treatment reveals a high number of paradoxical effects [8]. Investigating the regulation role of rapamycin on the effector leukocytes *in vivo* is of crucial importance to clarify this issue [2]. Immunohistochemistry and flow cytometry are the conventional approaches for investigating the behaviors and functions of immunocytes. However, these approaches only obtain static information from the immune cells at a given time in different individuals. It is difficult to represent the dynamic process of immunocytes and their function in microenvironments *in vivo* in the same individual. Thus, dynamically investigating the motility behaviors of neutrophils and MMs *in vivo* is useful for clarifying the immunosuppressant mechanism of rapamycin, which has not yet been reported.

Over the last decade, optical imaging techniques have become the main tools for intravital imaging because of their advantage of high spatio-temporal resolution and multi-channel parallel detection [12-14]. Here, we used multi-scale optical imaging approaches to investigate the dynamics of an ovalbumin (OVA)-induced DTH reaction and the immunosuppressive effect of rapamycin. The mouse footpad, which is a classical model site of the DTH reaction [15, 16], was the site chosen for long-term non-invasive fluorescent imaging. The dynamics (e.g., recruitment, distribution, migration) of neutrophils and MMs, as well as the vascular permeability in the footpad, were monitored during the elicitation phase of the DTH reaction. The two polarized T helper subsets, Th1 and Th2, were identified by their cytokines, i.e., interferon  $\gamma$  (IFN- $\gamma$ ), interleukin 4 (IL-4), and transforming growth factor beta (TGF- $\beta$ ). Our multi-scale optical imaging data revealed how rapamycin treatment regulates the dynamics of neutrophils and MMs in a DTH reaction *in vivo*.

## Materials and methods

### Mice

C57BL/6 mice expressing EGFP under the control of the endogenous *Cx3cr1* locus, abbreviated as CX<sub>3</sub>CR1-GFP mice [17], were purchased from Jackson Laboratory (B6.129P-Cx3cr1<sup>tm1Litt</sup>/J, Stock No. 005582)

and reproduced in the specific pathogen-free (SPF) animal facility of WNLO-HUST. Most of the CX<sub>3</sub>CR1-GFP cells were monocytes (~90%) [17-20]. Neutrophils were obtained from ten-week-old C57BL/6 mice, which were purchased from Shanghai Slaccas Laboratory Animal Co., Ltd. (Hunan, China). Mice were maintained under SPF conditions, and all experiments were performed according to the animal experiment guidelines of the Animal Experimentation Ethics Committee of HUST.

### Neutrophil purification and adoptive transfer

Neutrophils were purified by negative selection from the bone marrow of ten-week-old C57BL/6 mice using the MACS Neutrophil Isolation Kit and an autoMACS system (Miltenyi Biotec; Bergisch Gladbach, Germany). DiR-BOA [21] is a near-infrared fluorescent dye that has an excitation peak at 748 nm and an emission peak at 780 nm, which was gifted by Dr. Gang Zheng at University of Toronto, Canada. For whole-field fluorescent imaging, a total of  $2 \times 10^7$  neutrophils labeled with DiR-BOA in 300  $\mu$ l PBS were injected into CX<sub>3</sub>CR1-GFP mice via the tail vein 30 min before aggregated OVA (AOVA) challenge in the footpad [21]. For large-scale scanning microscopy and time-lapse confocal imaging, neutrophils labeled with eFluor670 dye (eBioscience, San Diego, CA, USA) were injected into CX<sub>3</sub>CR1-GFP mice via the tail vein.

### OVA-induced DTH reaction at footpad

AOVA was prepared by heating a 2% solution of OVA in physiological (0.15 M) saline [22]. To induce a DTH reaction, five- to six-week-old CX<sub>3</sub>CR1-GFP mice were immunized with 50  $\mu$ g OVA emulsified in 20  $\mu$ l complete Freund's adjuvant (CFA) by subcutaneous injection on both sides of the tail base. Seven days later, 30  $\mu$ l 2% AOVA was subcutaneously injected into the center of the right hind footpad, which was surrounded with six skin bulges (Supplementary Material: Fig. S1), and 30  $\mu$ l PBS was injected into the other hind footpad as a control. The thickness of the footpad was measured with calipers at the indicated time points (before antigen challenge and at 4, 24, 48, and 72 h post-challenge). The increase percentage of footpad thickness was calculated as follows: (%) = (Thickness<sub>after AOVA challenge</sub> - Thickness<sub>before challenge</sub>) / Thickness<sub>before challenge</sub>  $\times$  100%. For tissue section analysis, mice were euthanized at 48 h after AOVA challenge. The paws of mice were dissected and fixed in 10% formalin in PBS for H&E staining and analysis.

### Rapamycin treatment

Rapamycin (Sigma, St. Louis, MO, USA) was dissolved in DMSO and then suspended in 0.5% sodium carboxymethyl cellulose to prepare the solution

at working concentrations of 0.3, 1, 3, and 10 mg/ml. Aside from the 7<sup>th</sup> day, rapamycin was injected intraperitoneally once daily for nine days, beginning on the day of OVA sensitization. At day 7, rapamycin was administered three times: the 1<sup>st</sup> time was at 1 h before antigen challenge, the 2<sup>nd</sup> time was immediately after antigen challenge, and the 3<sup>rd</sup> time was at 3 h after antigen challenge [23, 24].

### Whole-field fluorescent imaging

Footpads of mice were treated with depilatory cream and exfoliating cream one day before AOVA challenge. Mice were anesthetized intraperitoneally with 0.2 mg ketamine/g body weight and 0.02 mg xylazine/g body weight. A home-made whole-field fluorescent imaging system [25-27] with a xenon lamp and a cooled CCD (Coolsnap ES2, Photometrics, Tucson, Arizona, U.S.A.) was used to image the recruitment of neutrophils and MMs in the whole footpad. The BP469/40 excitation filter and BP510/40 emission filter were used for imaging CX<sub>3</sub>CR1-GFP MMs. The BP716/40 excitation filter and BP800/40 emission filter were used for imaging DiR-BOA-labeled neutrophils. Image analysis and processing were performed using the ImageJ software (<http://rsb.info.nih.gov/ij/>). The fluorescence intensity (FI) of neutrophils and MMs were obtained from the 'imaging area' (Supplementary Material: Fig. S1) inside the six skin bulges at the footpad, which avoided the noise signal interference from the skin bulges. Inhibition ratio =  $(FI_{AOVA} - FI_{AOVA+Rapamycin}) / FI_{AOVA}$ .

### Intravital microscopy

For large-scale scanning microscopy in the footpad, a Nikon A1 Ti laser scanning confocal microscope (Nikon Co., Japan) with an inverted 20×/0.75 objective and 34.2 μm pinhole was used to detect the GFP signal (488 nm laser, 500-550 nm emission) and the eFluor 670 signal (638 nm laser, 650-700 nm emission). Large-scale images were a composite of 8 × 6 frames (645 × 645 μm/frame, 2.2 μs/pixel) with 15% overlap. An Olympus FV1000 scanning confocal microscope (Olympus Optical Co., Ltd, Japan) with an inverted 20×/0.75 objective and 200 μm pinhole was used to acquire the time-lapse images by scanning 636 × 636 μm/frame (8 μs/pixel) without intervals. The depth of the dermis was 22-50 μm (Supplementary Material: Fig. S2), which was indicated by the second harmonic generation (SHG) signal [28]. We chose an imaging layer at a depth of 50 μm below the outermost epidermal layer to obtain a high density of immunocyte signals. Image analysis and processing were performed using ImageJ software.

### Data analysis of the distribution of neutrophils and MMs in inflammatory foci during the DTH reaction

Firstly, the 'imaging area' inside the region of the six skin bulges was draw out from the whole images, as detected using large-scale scanning microscopy. Secondly, the 'imaging area' (Supplementary Material, left images of Fig. S3A and S3B) was divided into 2,200 sub-areas (50 × 50 μm/subareas, right images of Fig. S3A and S3B). Next, the average fluorescence intensity of each sub-area was obtained using the ImageJ software, and the percentages of sub-areas at different levels of average fluorescence intensity (100/level) was presented using the Graphpad Prism software (Supplementary Material: Fig. S3C). Finally, a comprehensive analysis of sub-areas distribution percentages of leukocytes at different time points was performed, with sub-areas that had an average fluorescence intensity equal to or greater than 300 were set as the positive subareas. The inhibition ratio was calculated as follows:  $(Subareas_{AOVA} - Subareas_{AOVA+Rapamycin}) / Subareas_{AOVA}$ .

### Data analysis of the motility parameters of neutrophils and MMs

The motility parameters of neutrophils in the footpad of AOVA-challenged mice were extracted from the time-lapse images and characterized as follows [29-31]: 1) Mean velocity (MV): Mean velocity of a cell over several time steps (usually the entire imaging period), μm/min; 2) Arrest coefficient (AC): the proportion of time for which an individual cell remains arrested. The time during which each cell's instantaneous velocity is below 2 μm/min/total time; 3) Migration displacement (MD): Straight-line distance of a cell from its starting point after any given time, μm; 4) Confinement ratio (CR): Displacement/path length for a given time interval (a measure of cell directionality); and 5) Mean displacement plots (MDP): Displacement (μm) vs. squared root time (min<sup>1/2</sup>) shows a strong linear correlation indicative of random cell migration; a curve upward represented directed migration, while a transition from a linear relationship to a plateau represented constrained motility. The motility parameters for the immunocytes recorded using confocal microscope were analyzed using the Image-Pro Plus software and the ImageJ software.

### Water-soluble quantum dot (QD) and Evans blue injection for verification of the vascular hyperpermeability

CdSe QDs without any modification and functional coating (Wuhan Jiayuan Quantum Dots Co., LTD., China) were used to synthesize the wa-

ter-soluble QD according to previously reported studies [32]. Water-soluble QD solution (10 mg/kg) in 300  $\mu$ l PBS or Evans blue (100 mg/kg) [33] in 500  $\mu$ l PBS was intravenously injected at the indicated time points 10 min before imaging acquisition.

### ELISA analysis of cytokines

Blood was collected from the retro-orbital sinus before AOVA challenge and at 4 and 24 h post-challenge. All sera were collected and stored at  $-80^{\circ}\text{C}$  for ELISA analysis of the cytokines IFN- $\gamma$ , IL-4, and TGF- $\beta$  (Cytokine ELISA kits, Dakewe Biotech CO., LTD., Beijing, China). All procedures were conducted according to the manufacturer's protocols.

### Statistical analysis

Experimental data were expressed as the mean  $\pm$  SEM. Histograms were presented using the Graphpad Prism software. Two-way ANOVA analysis and Bonferroni post-tests were used for statistical analysis between the AOVA group and the AOVA + Rapamycin group at the same time point, and one-way ANOVA analysis and Bonferroni post-tests were used for statistical analysis between the different time points. The statistical analysis is described in each figure legend. Significant differences between or among groups were indicated by ns for non-significant, \* for  $P < 0.05$ , \*\* for  $P < 0.01$ , and \*\*\* for  $P < 0.001$ , respectively.

## Results

### AOVA-elicited DTH reaction and footpad swelling attenuated by rapamycin treatment

In the mouse model of an AOVA-elicited DTH reaction, footpad swelling occurred at 4 h post-challenge, with  $31.9 \pm 3.8\%$  incassation, reached its maximum at 48 h, with  $80.6 \pm 6.4\%$  incassation, and then decreased to  $52.8 \pm 7.5\%$  incassation at 72 h post-challenge (Figs. 1A and 1B). Rapamycin treatment could readily inhibit the DTH reaction in a dose-dependent manner (Fig. 1B). Compared to the AOVA challenge alone at 48 h, which was the maximum footpad swelling time-point, a high dosage of 10 mg/kg rapamycin significantly inhibited footpad edema, with only  $34.7 \pm 3.3\%$  incassation ( $P < 0.001$ ,  $n = 6$ ). In addition, 3.0 mg/kg rapamycin treatment inhibited DTH, with  $42.4 \pm 3.1\%$  incassation ( $P < 0.001$ ,  $n = 6$ ), and a 1.0 mg/kg rapamycin treatment appeared to weakly inhibit DTH, with  $59.7 \pm 6.9\%$  incassation ( $P > 0.05$ ,  $n = 6$ ), but a low dose of rapamycin (0.3 mg/kg) could not inhibit the footpad swelling ( $P > 0.05$ ,  $n = 6$ , Figs. 1A and 1B). Thus, a 10 mg/kg dose of rapamycin was used in subsequent experiments. Consistent with footpad incassation, the histological analysis of footpad tissues confirmed the mass infiltration of inflammatory cells and edema in the epidermis and dermis at 48 h in the AOVA challenge group and a lesser infiltration of inflammatory cells in rapamycin-treated mice (Supplementary Material: Fig. S4).

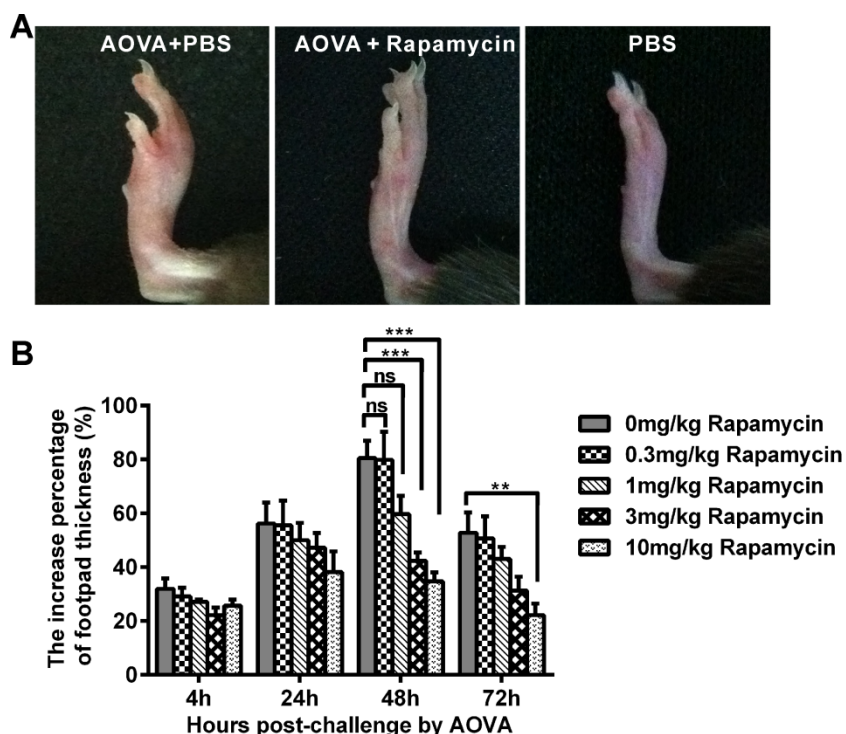


**Figure 1.** AOVA-elicited footpad swelling and the immunosuppressive effect of rapamycin. A) Photos of footpad swelling at 48 h in CX<sub>3</sub>CR1-GFP mice. Left: AOVA elicitation and PBS treatment; Middle: AOVA elicitation combined with rapamycin treatment; Right: PBS treatment as negative control. B) Histogram of the degree of footpad swelling. Mean values  $\pm$  SEM (The data were from 6 mice per group). Two-way ANOVA and Bonferroni post-tests were used for statistical analysis between the AOVA group and the AOVA + Rapamycin group at the same time point.

### Whole-field fluorescent imaging for the recruitment of neutrophils and MMs in the AOVA-challenged footpad

It was previously reported that rapamycin inhibits the adherence and chemotaxis of MMs and neutrophils *in vitro* [9, 10]. We speculated that the significant inhibition of edema by rapamycin (10 mg/kg) during a DTH reaction occurred because of the blocking the recruitment of neutrophils and MMs at the antigen challenge site. To visualize the recruitment of neutrophils and MMs in the AOVA-challenged footpad and to evaluate the inhibition efficiency of rapamycin, whole-field fluorescent imaging for the same individual was performed at the indicated time points [34]. As shown in Figure 2, the footpad did not appear to have an obvious increase in fluorescent signals at 4 h post-challenge. After 24 h, the fluorescence intensity of DiR-BOA and GFP in the footpad were remarkably increased (Figs. 2A and 2B), indicating the involvement of neutrophils and MMs during AOVA-elicited footpad swelling. Whole-field imaging data showed that rapamycin readily inhibited the recruitment of neutrophils and MMs, as the inhibition ratios for neutrophils were 69.4% at 24 h ( $P < 0.001$ ), 75.8% at 48 h ( $P < 0.001$ ), and 77.2% at 72 h ( $P < 0.001$ ) ( $n = 5$ , Fig. 2C), and the inhibition ratios for MMs were 54.1% at 24 h ( $P < 0.05$ ), 47.6% at 48 h ( $P < 0.01$ ), and 38.4% at 72 h ( $P < 0.01$ ) ( $n = 6$ , Fig. 2D). Notably, in the rapamycin-treated mice at 24 h after AOVA challenge, the fluorescent signal of neutrophils remained unchanged, but the inhibition ratio was increased; however, the MM signal continued to rise, and the inhibition ratio decreased. These data suggest that neutrophils are mainly involved in the early stage of an inflammation reaction and MMs play key roles in the late stage.

### Evaluating the effect of rapamycin on the distribution of neutrophils and MMs in inflammatory foci using large-scale scanning microscopy

To observe the dynamic recruitment and distribution of neutrophils and MMs and to evaluate the inhibition efficiency of rapamycin in the antigen challenge site at the cellular level, intravital large-scale scanning microscopy was used to collect the fluorescent signals in the dermis of the footpad. The imaging area of the large-scale scanning microscopy was located inside the region of the six skin bulges. For quantitatively describing the cell distribution, the whole 'imaging area' was divided into 2,200 sub-areas ( $50 \times 50 \mu\text{m}/\text{subarea}$ ) [35, 36]. The sub-areas with an intensity above a particular average fluorescence intensity were considered the positive subareas,

indicating that the fluorescent-labeled neutrophils and MMs were located there. Thus, the distribution of neutrophils and MMs was plotted against the percentage of positive subareas based on the time elapsed since AOVA challenge [36]. The inhibition ratio was calculated as follows:  $(\text{Subareas}_{\text{AOVA}} - \text{Subareas}_{\text{AOVA+Rapamycin}}) / \text{Subareas}_{\text{AOVA}}$ .

As shown in Figures 3A and 3B, at 4 h post-challenge, few eFluor670-labeled neutrophils and GFP-expressing CX<sub>3</sub>CR1<sup>+</sup> MMs appeared in both the AOVA-injected footpad and the opposite footpad. At 24 h post-challenge, both neutrophils and MMs were obviously recruited and formed high-intensity clusters at the site of AOVA injection with small areas ( $31.2 \pm 6.3\%$  for neutrophils,  $21.9 \pm 3.6\%$  for MMs,  $n = 6$ ). The imaging data at 48 and 72 h showed that the immunocytes expanded from the initial cluster area to the vicinity and filled the whole region in the footpad as the reaction progressed. The positive subareas of neutrophils filled  $45.9 \pm 4.9\%$  of the region at 48 h and  $48.4 \pm 5.9\%$  at 72 h (Fig. 3C), while the positive subareas of MMs accounted for  $48.7 \pm 5.1\%$  of the region at 48 h and  $65.5 \pm 2.6\%$  at 72 h (Fig. 3D). Thus, this result also indicates that the response of the neutrophils was earlier and more rapid than that of the MMs during the DTH reaction.

Rapamycin treatment obviously attenuated the AOVA-induced DTH reaction, with slight footpad swelling (Fig. 1) and inhibited the recruitment of MMs and neutrophils (Fig. 2). Using large-scale scanning microscopy, we unexpectedly found that neutrophils were recruited to the footpad early in rapamycin-treated mice (Fig. 3B), and this recruitment was not revealed by whole-field imaging. At 4 h post-challenge, neutrophils appeared in  $15.7 \pm 3.6\%$  of the total area in the footpad of rapamycin-treated mice but only appeared in  $2.2 \pm 0.2\%$  of the area in the footpad of the mice with a classic DTH reaction (Fig. 3C,  $P < 0.01$ ,  $n = 6$ , unpaired t test). Compared to the DTH reaction group, rapamycin was successful at inhibiting the subsequent recruitment of neutrophils, as the positive subareas of neutrophils increased slightly to  $25.8 \pm 3.7\%$  at 24 h ( $P > 0.05$ ,  $n = 6$ ) and then decreased to  $22.5 \pm 4.1\%$  at 48 h ( $P < 0.01$ ) and  $22.6 \pm 4.5\%$  at 72 h ( $P < 0.001$ ). In contrast to the inhibitory effect of rapamycin on neutrophils, rapamycin inhibited the recruitment of MMs, with  $5.9 \pm 2.3\%$  of positive subareas at 24 h ( $P < 0.05$ ,  $n = 6$ ),  $24.5 \pm 4.8\%$  at 48 h ( $P < 0.001$ ), and  $35.6 \pm 7.2\%$  at 72 h ( $P < 0.001$ ) (Fig. 3D). In other words, the inhibitory effect of rapamycin on the recruitment of neutrophils was not significantly different compared to the DTH reaction group at 24 h; this effect then increased to 50.9% at 48 h and 53.3% at 72 h, whereas its inhibition ratio on the recruitment of MMs was decreased from 73.1% at 24 h

to 49.6% at 48 h and 45.6% at 72 h (Figs. 3C and 3D). These results further confirm that rapamycin induces the early recruitment of neutrophils and delays the

involvement of MMs at the early stage of a DTH reaction.

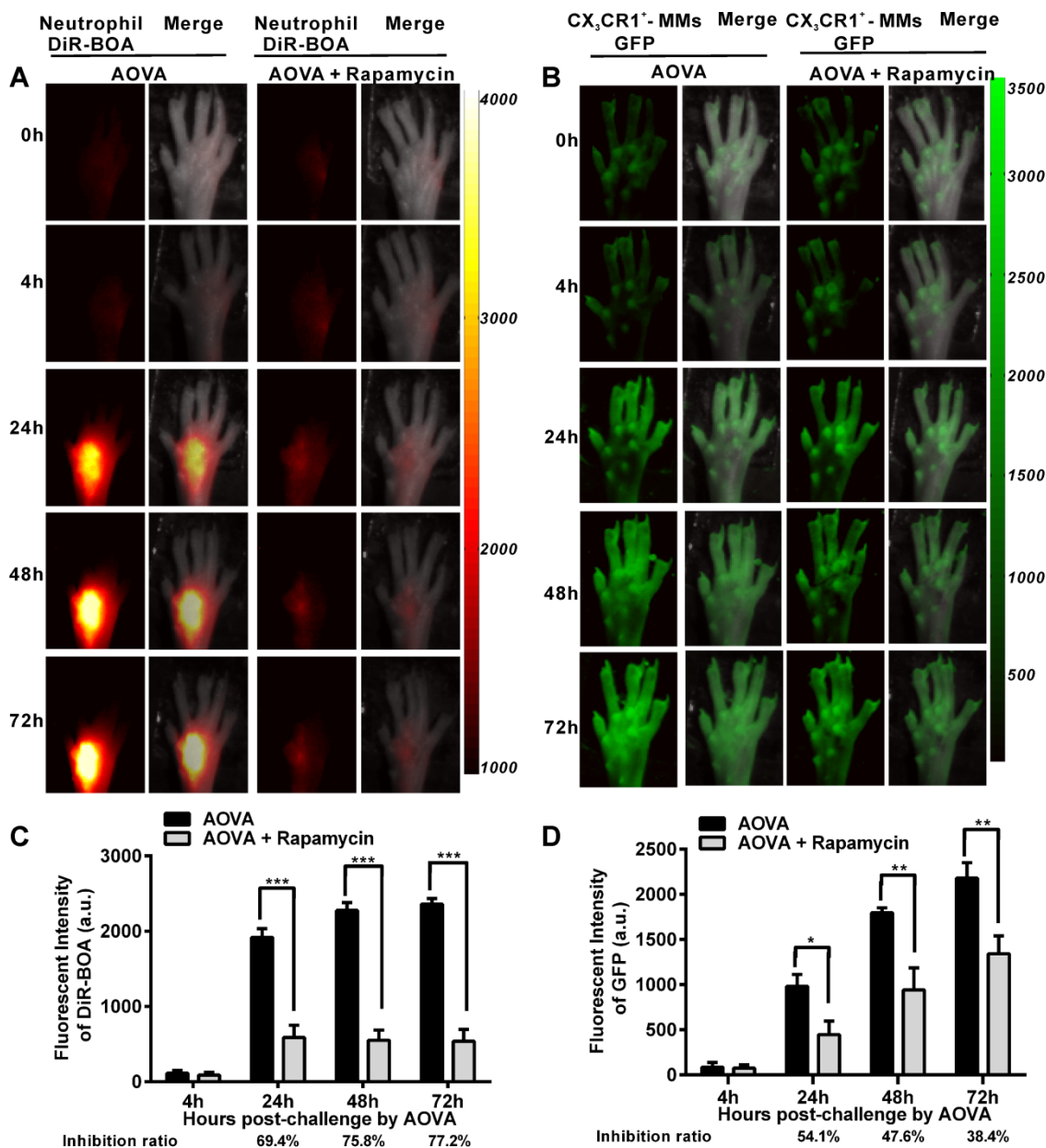


**Figure 2.** Whole-field fluorescent imaging for the recruitment of neutrophils and MMs in the footpad of AOVA-challenged mice. A-B) Representative fluorescent images showed the accumulation intensity of neutrophils (A, red signals) and MMs (B, green signals) during the DTH reaction with or without rapamycin treatment. C-D) Histogram of the average fluorescent intensity (FI) of neutrophils (C) and MMs (D). Mean values  $\pm$  SEM (Data were pooled from 5 mice per group for neutrophils and 6 mice per group for MMs). Two-way ANOVA and Bonferroni post-tests were used for statistical analysis between the AOVA group and the AOVA + Rapamycin group at the same time point.

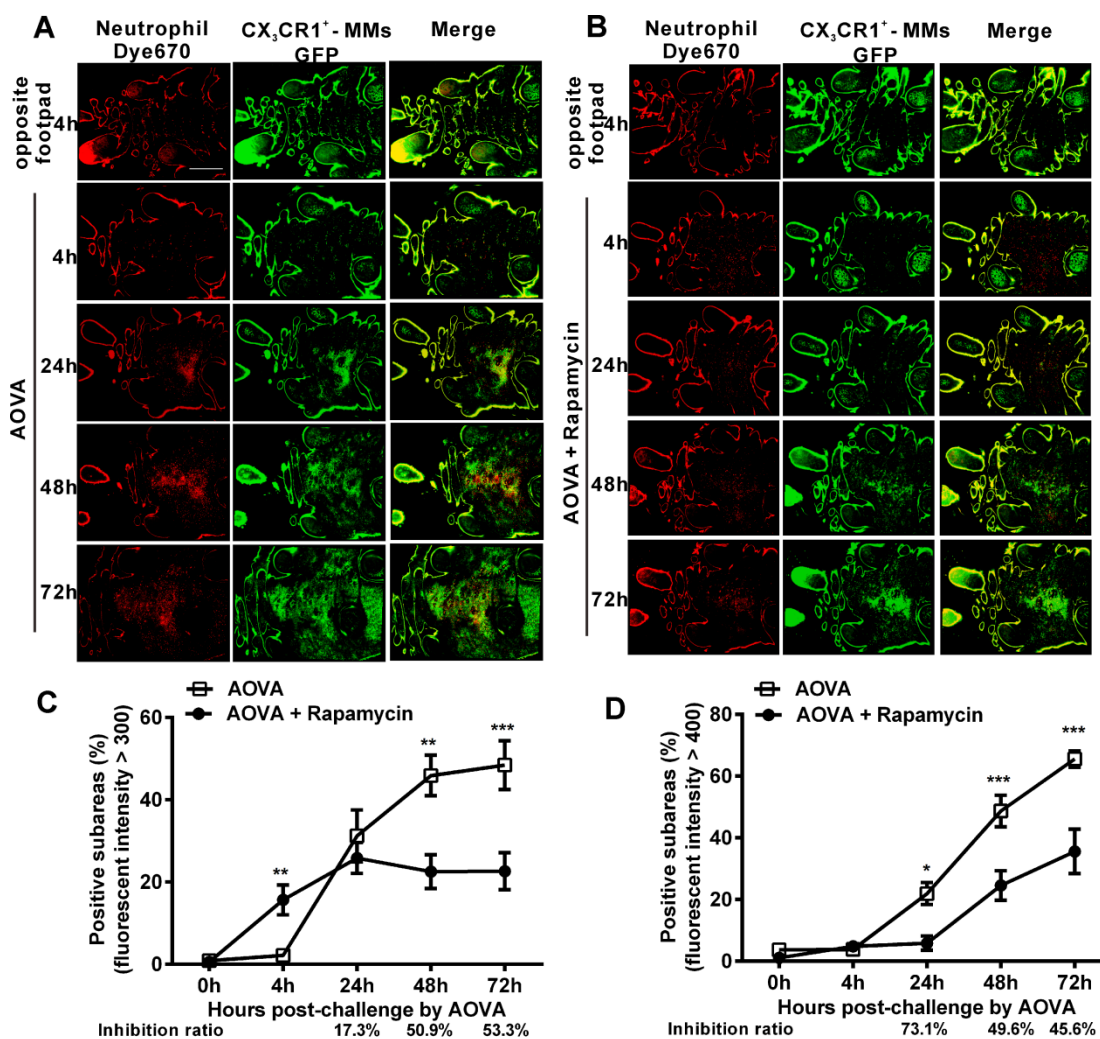


**Figure 3.** Large-scale scanning microscopy for the distribution of neutrophils and MMs in inflammatory foci of the DTH reaction and evaluation of the effect of rapamycin. A-B) Representative intravital fluorescent images of neutrophils (red) and MMs (green) in the footpad after AOVA elicitation with (B) or without (A) rapamycin treatment. Scale bar = 1000  $\mu$ m. C-D) The distribution of neutrophils (C) and MMs (D) is depicted by plotting the percentage of positive subareas against the number of hours following AOVA challenge. Mean values  $\pm$  SEM (Data were pooled from 6 mice per group). Two-way ANOVA and Bonferroni post-tests were used for statistical analysis between the AOVA group and the AOVA + Rapamycin group at the same time point. Specially, an unpaired t test was used for statistical analysis between the AOVA group and the AOVA + Rapamycin group at 4 h.

### Time-lapse confocal imaging of the migration of neutrophils in antigen-challenged foci

To evaluate the motility of neutrophils in antigen-challenged foci, the dynamics of immunocytes were measured with time-lapse confocal imaging and characterized by a series of parameters (Figs. 4A-4F). The mean velocity (MV) of the immunocytes decreased from an initial 6.95  $\mu$ m/min at 4 h to 5.79  $\mu$ m/min at 24 h, 4.89  $\mu$ m/min at 48 h, and 4.68  $\mu$ m/min at 72 h (Fig. 4B). In contrast, the arrest coefficient (AC) increased from 0.17 at 4 h to 0.23 at 24 h, 0.26 at 48 h and 0.30 at 72 h, indicating that the arrest duration was extended (Fig. 4C). The migration displacement (MD) of the cells decreased from 4 h to 72 h (Fig. 4D), and the confinement ratio (CR) gradually decreased from 0.39 at 4 h to 0.27 at 24 h, 0.08 at 48 h, and 0.07 at 72 h, indicating that the limitation of cell

movement gradually increased (Fig. 4E). Mean displacement plots (MDPs) were fitted with a straight line at 4 h, 48 h, and 72 h, indicating random migration at these time points; the MDPs went upward at 24 h, indicating the chemotactic migration of neutrophils (Fig. 4F). Thus, during the elicited phase of the DTH reaction, the migration features of neutrophils changed from rapid, random, and nonrestrictive migration at the early stage (4 h) to slower, restrictive, and chemotactic migration at the middle stage (24 h), and finally to slow and short mean displacement, severely restricted, and random migration at the late stage (48 h-72 h). Additionally, during the late stage, the morphology of neutrophils was abnormal, and the fluorescent dye leaked out from neutrophils, indicating the death of neutrophils after finishing their function.

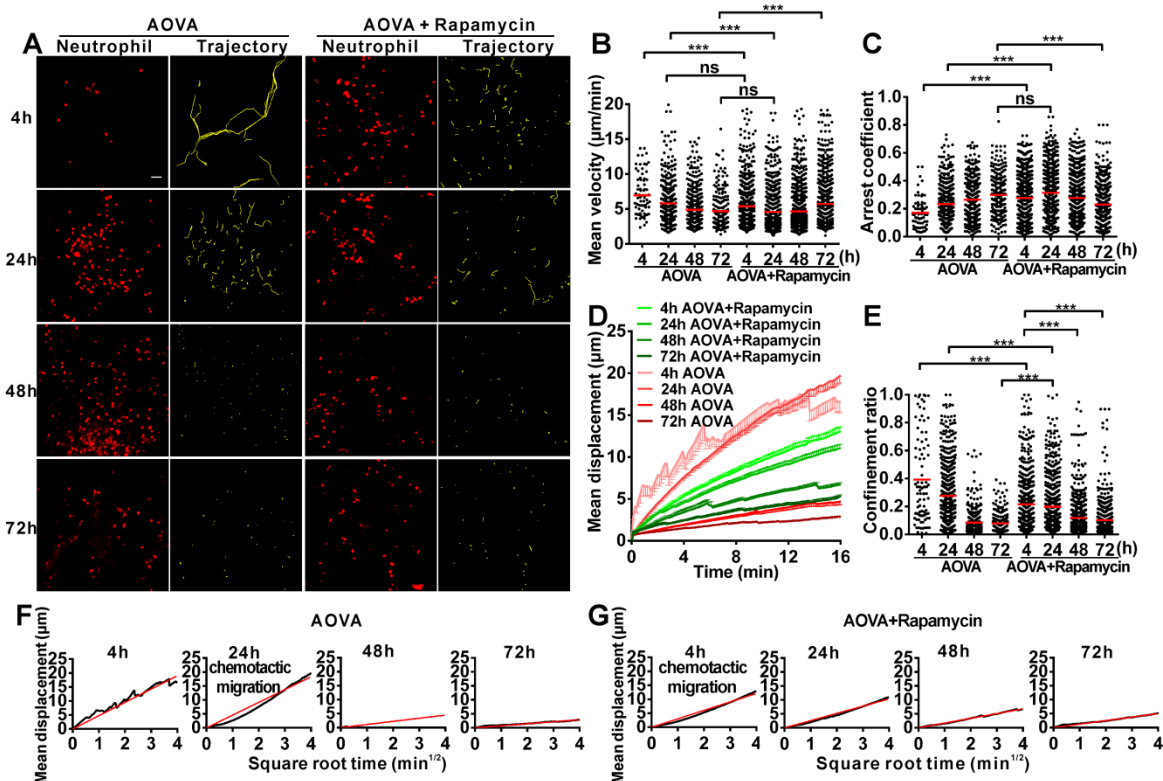


**Figure 4.** Time-lapse confocal imaging of the migration of neutrophils in the inflammatory foci of the DTH reaction and evaluation of the effect of rapamycin. A) Snapshot from intravital time-lapse images, including the motion trajectory of the neutrophils. Scale bar = 50  $\mu\text{m}$ . B-G) Motility parameters of neutrophils in the DTH reaction with or without rapamycin treatment. Each circle represents a cell (Data were pooled from 4 mice per group). B) Mean velocity ( $\mu\text{m}/\text{min}$ ), C) Arrest coefficient, D) Mean displacement ( $\mu\text{m}$ ), E) Confinement ratio, F-G) Displacement ( $\mu\text{m}$ ) vs. Square root of time ( $\text{min}^{1/2}$ ) for neutrophils with (G) or without (F) rapamycin treatment (black line). Red line: reference line. One-way ANOVA and Bonferroni post-tests were used for statistical analysis between the different time points.

The motility parameters of neutrophils were severely changed by rapamycin treatment (Figs. 4A-4G). Compared to the classic DTH reaction, at 4 h post-challenge, neutrophils displayed decreased MV (5.37  $\mu\text{m}/\text{min}$ ,  $P < 0.001$ ,  $n = 4$ ), increased arrest duration (AC = 0.27,  $P < 0.001$ ), more restricted (CR = 0.21,  $P < 0.001$ ), and slight chemotactic migration (Fig. 4G). At 24 h post-challenge, the MV of neutrophils was significantly decreased to 4.57  $\mu\text{m}/\text{min}$ , and the AC was increased to 0.31. Cell migration was more restricted (CR = 0.19) and displayed random movement, and from 48 h to 72 h, the MV of neutrophils increased again from 4.68  $\mu\text{m}/\text{min}$  at 48 h to 5.71  $\mu\text{m}/\text{min}$  at 72 h. The arrest duration was reduced, with an AC of 0.27 at 48 h and 0.22 at 72 h. Neutrophil motility also had a shortened mean displacement, increased restriction (the CRs at 48 h and 72 h were 0.11 and 0.10, respectively), and a random migration pattern. These results indicate that rapamycin treatment advanced the process of the DTH reaction at the early stage, with a similar mean velocity and chemotaxis observed for the classic DTH reaction at 24 h and the rapamycin-treated reaction at 4 h post-challenge by AOVA ( $P > 0.05$ ,  $n = 4$ , Fig. 4B). At 24 h post-challenge, neutrophils migration was restricted

in the rapamycin-treated reaction, which displayed a similar MV ( $P > 0.05$ , Fig. 4B) and arrest duration ( $P > 0.05$ , Fig. 4C) to that of a 72 h DTH reaction, but their MD and CR were significantly different ( $P < 0.001$ ). There was no visible leaked fluorescent dye from neutrophils in the rapamycin-treated reaction, even at 72 h post-challenge. These data suggest that the restrictive migration of neutrophils at the late stage resulted from environmental factors and was not due to cell death.

### Time-lapse confocal imaging of the migration of MMs in the antigen-challenged foci

We also obtained time-lapse images of MMs and extracted their motility parameters in the DTH reaction with or without rapamycin treatment (Fig. 5A). The MV of MMs was 7.47  $\mu\text{m}/\text{min}$  at 4 h and decreased to 6.12  $\mu\text{m}/\text{min}$  at 24 h (Fig. 5B). The AC of MMs was 0.17 at 4 h and then increased to 0.22 at 24 h (Fig. 5C). The MV and arrest duration of MMs at 48 h and 72 h were similar to those observed at 24 h. During the DTH reaction, the MD was gradually shortened (Fig. 5D), and the migration was more and more restrictive, as represented by the decreasing slope of MDP from 24 h to 72 h, especially displaying the con-

finer migration at 72 h (Fig. 5F). Thus, the migration of MMs in the DTH reaction was rapid, random, and nonrestrictive at 4 h in the early stage and slower and with an extended arrest duration in the middle- and late stages; migration was confined at 72 h.

Rapamycin treatment altered the migration of MMs in the AOVA-challenged reaction (Figs. 5A-5G). Compared to the features observed in the DTH reaction, the MV of MMs in the rapamycin treatment groups was slowed to  $5.83 \mu\text{m}/\text{min}$  ( $P < 0.001$ ,  $n = 4$ , Fig. 5B) at 4 h and remained stable until 48 h; the AC of the MMs from 4 h to 48 h was similar to that observed in the DTH reaction group at 4 h ( $P > 0.05$ , Fig.

5C). At 24 and 48 h post-challenge, the MMs displayed an increased mean displacement (Fig. 5D), weakened restrictive movement (Fig. 5E), and remarkably confined migration (Fig. 5G). The motility of MMs in rapamycin-treated mice recovered at 72 h with rapid, nonrestrictive, and random migration. The data from the MMs also indicated that rapamycin treatment advanced the DTH reaction at the early stage, in which similar mean velocity and arrest duration were observed between the classic DTH reaction at 24 h and the rapamycin-treated reaction at 4 h post-challenge.

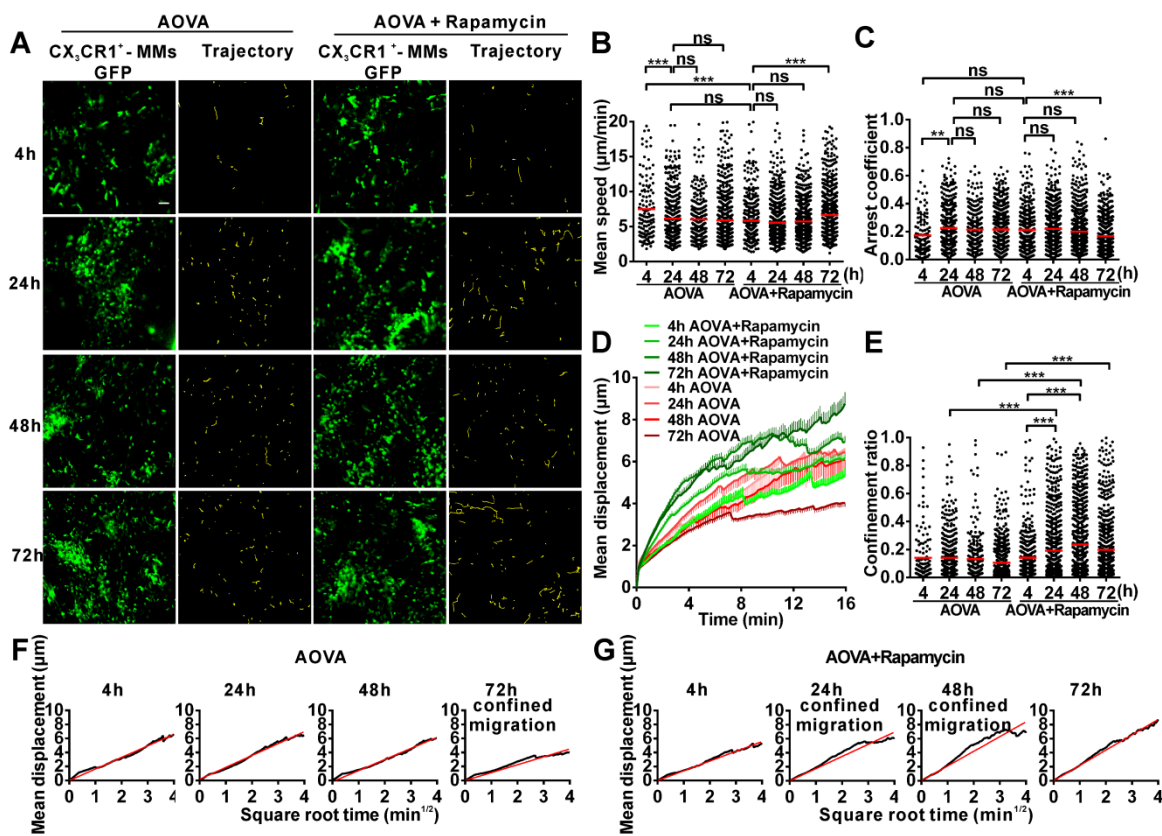


**Figure 5.** Time-lapse confocal imaging for the migration of MMs in the inflammatory foci of the DTH reaction and evaluation of the effect of rapamycin. A) Snapshot from intravital time-lapse images, including the motion trajectory of the MMs. Scale bar =  $50 \mu\text{m}$ . B-G) Motility parameters of MMs in the DTH reaction with or without rapamycin treatment. Each circle represents a cell (Data were pooled from 4 mice per group). B) Mean velocity ( $\mu\text{m}/\text{min}$ ), C) Arrest coefficient, D) Mean displacement ( $\mu\text{m}$ ), E) Confinement ratio, F-G) Displacement ( $\mu\text{m}$ ) vs. Square root of time ( $\text{min}^{1/2}$ ) for MMs with (G) or without (F) rapamycin treatment (black line). Red line: reference line. One-way ANOVA and Bonferroni post-tests were used for statistical analysis between the different time points.

### Verification of the vascular hyperpermeability in the AOVA challenge foci

Increased capillary permeability is an important event in the inflammatory response and may play an important role in leucocytes extravasations. To evaluate the modulation of the hyperpermeability of blood vessels during the DTH reaction by rapamycin treatment, water-soluble QDs ( $\sim 20 \text{ nm}$ ) were injected via the tail vein 10 min before performing vasculature

microscopy. The hair follicle was present in the imaging regions and displayed a strong autofluorescent signal. To quantify the permeability of the blood vessels, we used the ratio of the total fluorescence intensity of the QD [37] to the visible total length of the blood vessel in the imaging region, denoted as  $R_{\text{FI/LV}}$ , in which the autofluorescent signal from the hair follicle was subtracted.  $R_{\text{FI/LV}}$  was used to indirectly reflect the diameter change of the blood vessels. As shown in Figure 6A, the QD signal was weak before

the AOVA challenge. In the DTH reaction mice 4 h after antigen injection, the value of  $R_{FI/LV-4h}$  was increased 3.3-fold compared with  $R_{FI/LV-0h}$  ( $P < 0.05$ ,  $n = 3$ , Fig. 6B), but extravasation was not evident (Fig. 6A), indicating that the blood vessel swelled but was not permeable. At 24 h, a strong QD signal was observed in the blood vessel, displaying obvious extravasation; consistent with this, the value of  $R_{FI/LV-24h}$  increased by 7.4-fold compared with  $R_{FI/LV-0h}$  ( $P < 0.001$ ). At 48 and 72 h, the QD signal in the blood vessel was decreased, with  $R_{FI/LV-48h}$  and  $R_{FI/LV-72h}$  at 71.8% ( $P < 0.05$ ) and 60.3% of  $R_{FI/LV-24h}$  ( $P < 0.001$ ). In rapamycin-treated mice 4 h after antigen injection, we observed QD leakage from the blood vessel, and the value of  $R_{FI/LV-4h}$  was 1.5-fold higher than the  $R_{FI/LV-4h}$  value for

AOVA ( $P < 0.05$ ). The permeability of the blood vessel gradually recovered from 24 h to 72 h. To confirm this phenomenon, a traditional dye of Evans blue (100 mg/kg) was used to evaluate the permeability of the blood vessel [33]. Consistent with the QD-based vascular microscopy, the whole footpad appeared blue, thus indicating the occurrence of vascular hyperpermeability at 24 and 48 h post-challenge in DTH reaction mice and at 4 h post-challenge in rapamycin-treated mice (Fig. 6C). Thus, rapamycin treatment modulated the time of vascular hyperpermeability in the DTH reaction. This finding further confirms our viewpoint that rapamycin treatment shortens the DTH reaction process.

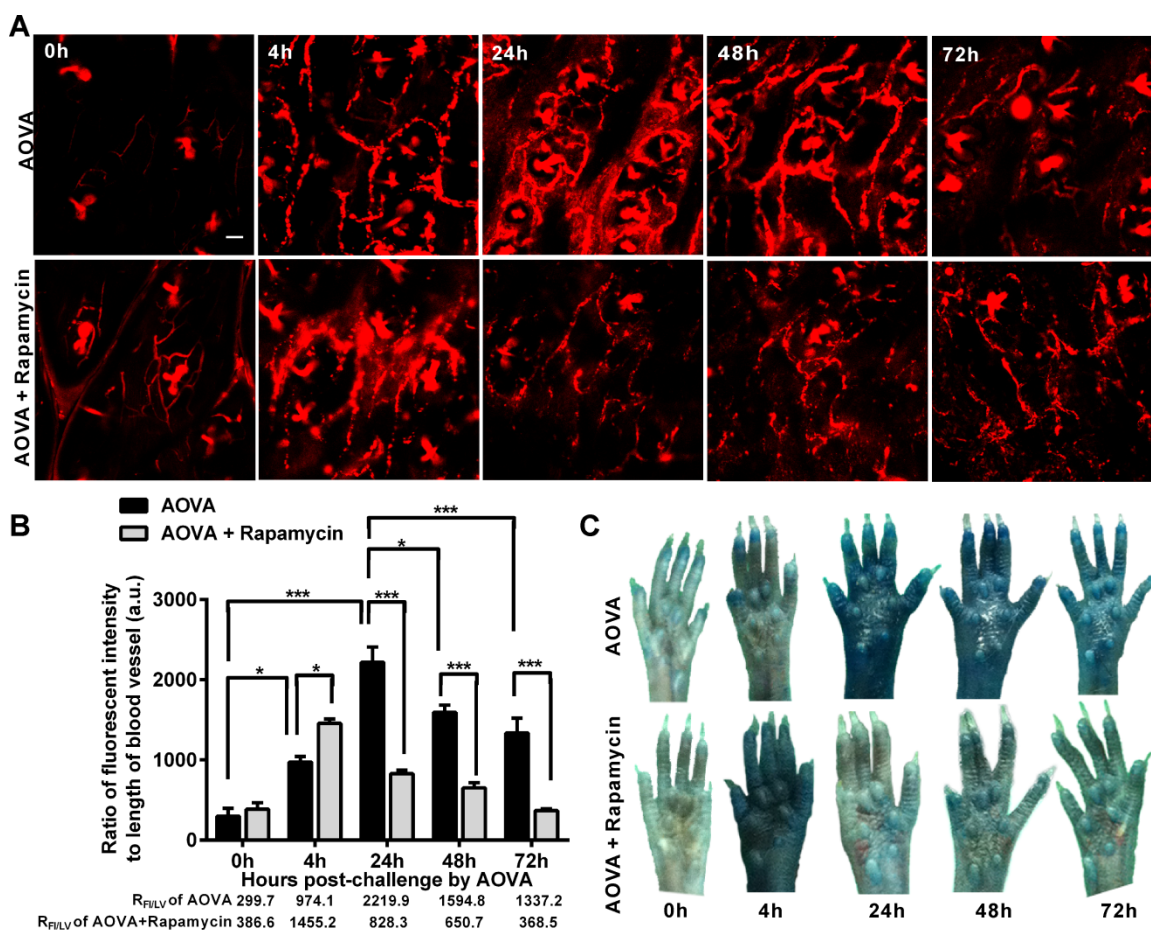


**Figure 6.** Verification of the vascular hyperpermeability in the inflammatory foci of the DTH reaction with or without rapamycin treatment. A) Representative intravital snapshot of blood vessels (red) after water-soluble QD injection. Scale bar = 50  $\mu$ m. B) The histogram of  $R_{FI/LV}$ . Mean values  $\pm$  SEM (Data were pooled from 3 mice per group). Two-way ANOVA and Bonferroni post-tests were used for statistical analysis between the AOVA group and the AOVA + Rapamycin group, and one-way ANOVA and Bonferroni post-tests were used for statistical analysis between the different time points (0, 4, 24, 48, and 72 h). C) Evaluation of the blood vessel permeability by the i.v. injection of Evans Blue.

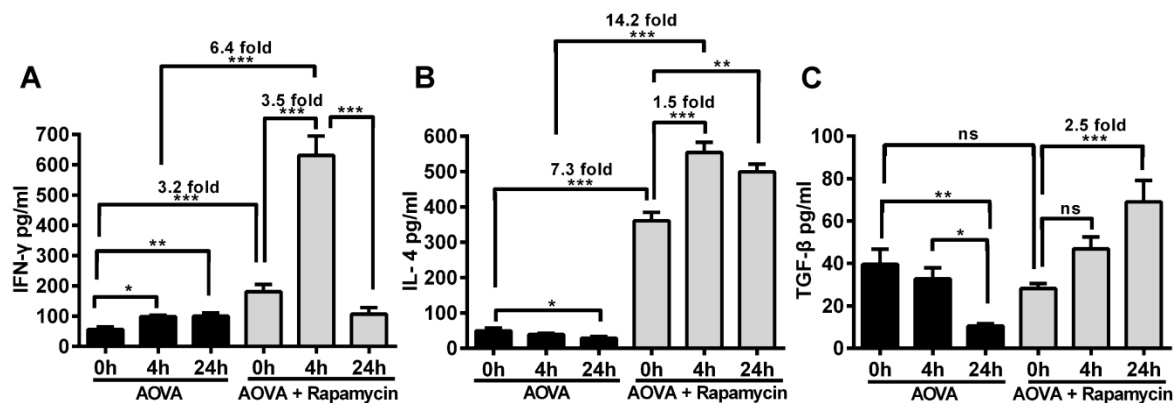


**Figure 7.** ELISA analysis of IFN- $\gamma$ , IL-4 and TGF- $\beta$  levels in the blood serum from the DTH reaction mice before and after 4 and 24 h of AOVA challenge with or without rapamycin treatment. Mean values  $\pm$  SEM (Data were pooled from 4 mice per group). Two-way ANOVA and Bonferroni post-tests were used for statistical analysis between the AOVA group and the AOVA + Rapamycin group, and one-way ANOVA and Bonferroni post-tests were used for statistical analysis between the different time points (0, 4, and 24 h).

### Measurement of cytokines to determine the effect of rapamycin on T cell polarization in the DTH reaction

The concentrations of IFN- $\gamma$ , IL-4 and TGF- $\beta$  in the serum were measured before and after 4 h and 24 h of AOVA challenge (Figs. 7A-7C). The DTH reaction was polarized in a Th1 response [38], as illustrated by the gradual up-regulation of the IFN- $\gamma$  level ( $56.4 \pm 8.2$  pg/ml at 0 h,  $98.6 \pm 4.8$  pg/ml at 4 h, and  $99.6 \pm 11.0$  pg/ml at 24 h) and the gradual down-regulation of IL-4 ( $49.3 \pm 7.5$  pg/ml at 0 h,  $39.1 \pm 3.4$  pg/ml at 4 h, and  $28.8 \pm 4.3$  pg/ml at 24 h) and TGF- $\beta$  levels ( $39.6 \pm 7.1$  pg/ml at 0 h,  $32.8 \pm 5.1$  pg/ml at 4 h, and  $10.5 \pm 1.1$  pg/ml at 24 h). We found that the expression of all three types of cytokines was significantly increased in rapamycin-treated mice, in which the initial concentrations of IFN- $\gamma$  and IL-4 were 3.2- and 7.3-fold higher ( $P < 0.001$ ,  $n = 4$ ), respectively, than those observed in the classic DTH reaction mice before AOVA challenge. However, the initial concentration of TGF- $\beta$  in rapamycin-treated mice was not significantly different from the DTH reaction mice before the AOVA challenge. At 4 h post-challenge, all three cytokines were increased. In particular, IFN- $\gamma$  ( $630.9 \pm 63.8$  pg/ml) was increased 3.5-fold ( $P < 0.001$ ) over its initial concentration in rapamycin-treated mice and 6.4-fold ( $P < 0.001$ ) over its level in DTH reaction mice at 4 h. At 24 h post-challenge, IFN- $\gamma$  ( $106.4 \pm 22.0$  pg/ml) was sharply down-regulated with 83% attenuation, thus displaying a similar concentration between rapamycin-treated and DTH reaction mice. Meanwhile, IL-4 remained at a high level of expression from 4 to 24 h, displaying a 1.5-fold ( $P < 0.001$ ) increase compared to its initial concentration in rapamycin-treated mice and a 14.2-fold ( $P < 0.001$ ) increase compared to the level observed in DTH reaction mice at 4 h. The concentration of TGF- $\beta$  contin-

ued to increase from  $28.1 \pm 2.2$  pg/ml at 0 h to  $46.9 \pm 5.6$  pg/ml at 4 h and  $69.0 \pm 10.1$  pg/ml at 24 h ( $P < 0.001$ ) after AOVA challenge in rapamycin-treated mice. These results suggest that the inhibition of the DTH reaction by rapamycin is correlated with the involvement of Th2 cells and regulatory T cells, which are critical for the up-regulation of IL-4 and TGF- $\beta$  and the down-regulation of IFN- $\gamma$  [39]. We also presumed that an extremely high expression level of IFN- $\gamma$  at 4 h in rapamycin-treated mice was correlated with the polarization of the T cells in the microenvironment of the DTH reaction [40-42].

### Discussion

Intravital imaging approaches promote the dynamic investigation of cellular behaviors in the true microenvironment and in the same individual over a long time period [12, 43]. In this study, we used multi-scale optical imaging approaches to visually investigate and quantitatively describe how, when and where neutrophils and MMs became major effector cells in the elicitation phase of the DTH reaction. The footpad is an ideal location to study innate immune cell trafficking during the Th1 polarized immune response [15, 44, 45] and is a convenient place to perform the non-invasive intravital microscopy. Thus, we use the footpad DTH reaction model to investigate the effect of an immunosuppressant on innate immune cells *in vivo*.

To evaluate the spatio-temporal dynamic of the immune response from the whole field of footpad to the cellular level, the multi-scale optical imaging approaches that we used included whole-field fluorescent imaging, large-scale scanning microscopy, and time-lapse confocal imaging. The recruitment of leukocytes could be directly visualized using whole-field fluorescent imaging at the organ and tissue levels. The dynamic distribution of the leukocytes was directly

visualized using large-scale scanning microscopy at the single-cell level. The motility and migration dynamics of leukocytes were visualized in real time and analyzed using time-lapse confocal imaging at the single-cell level with high temporal resolution. At 4 h (the early stage of the DTH reaction), the accumulation intensities of both neutrophils and MMs were low, and the distribution areas were smaller, which is consistent with the findings of previous studies using flow cytometry or immunohistochemistry [22, 46]. The leukocytes underwent random migration, with high migration velocity, a low arrest coefficient, and large mean displacement. We speculated that the cells in the early stage were busy modifying the local microenvironment to prepare for the delayed intense reaction, and this process is critical for initiating a full DTH response [46]. The OVA-elicited DTH reaction is characterized as a Th1 cell immune response with apparent edema from 24 h to 72 h [38]. In our AOVA-elicited DTH reaction in the footpad, obvious tissue swelling appeared at 24 h, reached a peak at 48 h, and was maintained until 72 h. Along with severe tissue edema, abundant neutrophils and MMs accumulated in the antigen injection region at 24 h, which was mediated through the Th1 cell response via the increased IFN- $\gamma$  level and the decreased IL-4 and TGF- $\beta$  levels. Moreover, we verified that the local implantation of *E. coli* efficiently induced the recruitment of neutrophils and MMs but that rapamycin failed to inhibit the footpad swelling and the innate leukocytes recruitment (data not shown). Thus, rapamycin mainly affected the T cell response, thereby indirectly modulating the motility of the innate leukocytes in the AOVA-elicited DTH reaction. Increased capillary permeability is an important event in the inflammatory response and may play an important role in leukocyte extravasation. Our data showed that the accumulation of neutrophils and MMs in the AOVA-challenged footpad was proportional to the permeability of the blood vessels, indicating that neutrophils and MMs extravasated from the permeabilized blood vessels into the inflammatory foci. Neutrophils typically function to scavenge antigen [47] and to recruit effector lymphocytes and mononuclears [46, 48]. MMs also function to phagocytose [47], interact with T cells for antigen presentation [38], and regulate neutrophil extravasation [49]. Thus, the reduced mean velocity and increased arrest coefficient of the neutrophils and MMs from 24 h to 72 h are not surprising. In particular, at 72 h, the footpad displayed attenuated swelling and weakened vascular hyperpermeability, thus indicating that the DTH response faded. At this time point, the neutrophils slowed down, displayed a damaged morphology, and leaked dye, indicating that the neutrophils performed

their function and died [50]. The MMs also slowed down, but their accumulation intensity and area greatly increased, indicating that the MMs were functioning to clear the neutrophils and repair the tissue [51].

By targeting the mTOR signal pathway, rapamycin has been reported to inhibit macrophage adherence, chemotaxis and phagocytosis by inhibiting ROCK-1 synthesis in macrophages [9]. It also potently suppresses neutrophil polarity and chemotaxis via IL-8 in angioplasty inflammation [11] or by cAMP [10] and plays an important role in promoting regulatory T cells for immunological tolerance [39]. Our data showed that rapamycin extensively modulated the recruitment behaviors of neutrophils and MMs as well as vascular hyperpermeability and cytokine levels. At 4 h, rapamycin advanced the accumulation of neutrophils in the AOVA-challenged footpads. The MMs and neutrophils displayed a decreased mean migration speed and increased arrest duration, which were similar to those observed in the DTH reaction at 24 h, together with increased vascular permeability and cytokine expression levels (e.g., IFN- $\gamma$ , IL-4 and TGF- $\beta$ ), suggesting that rapamycin treatment shortened the initial preparatory stage of the DTH reaction and resulted in the attenuation of the intense DTH reaction. We presume that rapamycin treatment mediated the extremely high level of IFN- $\gamma$  at 4 h post-challenge and might play a key role in the polarization of T cells, as IFN- $\gamma$  not only induces the DTH response but may also be required for the involvement of Th2 cells [40-42]. At 24 h, rapamycin treatment resulted in reduced accumulation intensity, a small distribution area, and slowed motility of neutrophils and MMs and helped recover the integrity of the vascular walls, which was related to the continuously high levels of IL-4 and TGF- $\beta$  in the blood serum.

In addition to the dynamic investigation of the behaviors of neutrophils and MMs in the DTH reaction, further studies on the roles of T cells in the DTH reaction, including their location, activation, proliferation, and cell-cell contact, could be explored using these multi-scale optical imaging approaches.

## Conclusions

Using multi-scale optical imaging approaches, we directly visualized the dynamic modulatory effects of the immunosuppressant rapamycin on the behavior and functions of immune cells *in vivo*. Our intravital imaging data revealed that neutrophils respond earlier and faster than MMs and that these neutrophils are primarily involved in the early stage of the DTH reaction, while MMs play key roles in the late stage. Rapamycin treatment shortened the dura-

tion of the elicitation phase and attenuated the motility of neutrophils and MMs, resulting in a reduction in the number of accumulated neutrophils in inflammatory foci and diminished footpad swelling. Based on the cytokines profile, we speculate that the immunosuppressive mechanism of rapamycin is correlated with the involvement of regulatory T cells and the polarization of T cells to a Th2-type cell response.

## Acknowledgements

We thank Dr. Gang Zheng (University of Toronto, Toronto, ON, Canada) for providing DiR-BOA. We also thank the Optical Bioimaging Core Facility of WNLO-HUST for support in data acquisition, and the Analytical and Testing Center of HUST for spectral measurements.

This work was supported by the National Basic Research Program of China (Grant No. 2011CB910401), Science Fund for Creative Research Group of China (Grant No. 61121004), National Natural Science Foundation of China (Grant No. 81172153), National Science and Technology Support Program of China (Grant No. 2012BAI23B02), and Specific International Scientific Cooperation of China (Grant No.2010DFR30820).

## Supplementary Material

Figure S1. Imaging area for data analysis of the DTH reaction.

Figure S2. Distribution of GFP-expressing CX<sub>3</sub>CR1 cells and blood vessels in the footpad at 48 h post-challenge.

Figure S3. Data processing method of the distribution of neutrophils.

Figure S4. H&E stain of a cross-paw section of footpad at 48 h post-challenge.

<http://www.thno.org/v04p0201s1.pdf>

## Abbreviations

DTH: delayed type hypersensitivity; AOVA: aggregated ovalbumin; MMs: monocyte/macrophages; GFP: Green fluorescent protein; DiR-BOA: 1,1'-dioctadecyl-3,3,3',3'-tetramethylindotricarbocyanine iodide bisoleate; SHG: second harmonic generation; MV: Mean velocity; AC: Arrest coefficient; MD: Migration displacement; CR: Confinement ratio; MDP: Mean displacement plots; Th1: T helper type 1; Th2: T helper type 2; FI: fluorescent intensity; RFI/LV: total fluorescent intensity to the visible total length of blood vessel.

## Competing Interests

The authors have declared no competing interest exists.

## References

- López MN, Pereda C, Segal G, Muñoz L, Aguilera R, González FE, et al. Prolonged survival of dendritic cell-vaccinated melanoma patients correlates with tumor-specific delayed type IV hypersensitivity response and reduction of tumor growth factor  $\beta$ -expressing T cells. *J Clin Oncol.* 2009; 27: 945-52.
- Camirand G. New perspectives in transplantation through intravital microscopy imaging. *Curr Opin Organ Transplant.* 2013; 18: 6-12.
- Egen JG, Rothfuchs AG, Feng CG, Winter N, Sher A, Germain RN. Macrophage and T cell dynamics during the development and disintegration of mycobacterial granulomas. *Immunity.* 2008; 28: 271-84.
- Vocanson M, Hennino A, Rozieres A, Poyet G, Nicolas JF. Effector and regulatory mechanisms in allergic contact dermatitis. *Allergy.* 2009; 64: 1699-714.
- Greenberg JD, Reddy SM, Schloss SG, Kurucz OS, Bartlett SJ, Abramson SB, et al. Comparison of an in vitro tuberculosis interferon-gamma assay with delayed-type hypersensitivity testing for detection of latent *Mycobacterium tuberculosis*: a pilot study in rheumatoid arthritis. *J Rheumatol.* 2008; 35: 770-5.
- Momotani E, Ozaki H, Hori M, Yamamoto S, Kuribayashi T, Eda S, et al. *Mycobacterium avium* subsp. paratuberculosis lipophilic antigen causes Crohn's disease-type necrotizing colitis in Mice. *SpringerPlus.* 2012; 1: 47.
- Janes MR, Fruman DA. Immune regulation by rapamycin: moving beyond T cells. *Sci Signal.* 2009; 2: pe25.
- Ferrer I, Araki K, Ford M. Paradoxical aspects of rapamycin immunobiology in transplantation. *Am J Transplant.* 2011; 11: 654-9.
- Fox R, Nhan TQ, Law GL, Morris DR, Liles WC, Schwartz SM. PSGL-1 and mTOR regulate translation of ROCK-1 and physiological functions of macrophages. *EMBO J.* 2007; 26: 505-15.
- Liu L, Das S, Losert W, Parent CA. mTORC2 regulates neutrophil chemotaxis in a cAMP-and RhoA-dependent fashion. *Dev Cell.* 2010; 19: 845-57.
- Nührenberg TG, Voisard R, Fahlisch F, Rudelius M, Braun J, Gschwend J, et al. Rapamycin attenuates vascular wall inflammation and progenitor cell promoters after angioplasty. *FASEB J.* 2005; 19: 246-8.
- Germain RN, Robey EA, Cahalan MD. A decade of imaging cellular motility and interaction dynamics in the immune system. *Science.* 2012; 336: 1676-81.
- Pittet MJ, Weissleder R. Intravital imaging. *Cell.* 2011; 147: 983-91.
- QU J, LIU L, SHAO Y, NIU H, GAO BZ. Recent Progress in Multifocal Multiphoton Microscopy. *J Innov Opt Health Sci.* 2012; 5: 1250018.
- Zinselmeyer B, Lynch J, Zhang X, Aoshi T, Miller M. Video-rate two-photon imaging of mouse footpad—a promising model for studying leukocyte recruitment dynamics during inflammation. *Inflamm Res.* 2008; 57: 93-6.
- Konjufca V, Miller MJ. Two-photon microscopy of host-pathogen interactions: acquiring a dynamic picture of infection in vivo. *Cell Microbiol.* 2009; 11: 551-9.
- Khandoga AG, Khandoga A, Reichel CA, Bihari P, Rehberg M, Krombach F. In vivo imaging and quantitative analysis of leukocyte directional migration and polarization in inflamed tissue. *PLoS one.* 2009; 4: e4693.
- Swirski FK, Nahrendorf M, Eitzrodt M, Wildgruber M, Cortez-Retamozo V, Panizzi P, et al. Identification of splenic reservoir monocytes and their deployment to inflammatory sites. *Science.* 2009; 325: 612-6.
- Auffray C, Fogg D, Garfa M, Elain G, Join-Lambert O, Kayal S, et al. Monitoring of blood vessels and tissues by a population of monocytes with patrolling behavior. *Sci Signal.* 2007; 317: 666.
- Jung S, Aliberti J, Graemmel P, Sunshine MJ, Kreutzberg GW, Sher A, et al. Analysis of fractalkine receptor CX<sub>3</sub>CR1 function by targeted deletion and green fluorescent protein reporter gene insertion. *Mol Cell Biol.* 2000; 20: 4106-14.
- Larmann J, Frenzel T, Hahnenkamp A, Herzog C, Lorenz A, Steinbicker AU, et al. In vivo fluorescence-mediated tomography for quantification of urokinase receptor-dependent leukocyte trafficking in inflammation. *Anesthesiology.* 2010; 113: 610-8.
- Titus RG, Chiller JM. A simple and effective method to assess murine delayed type hypersensitivity to proteins. *J Immunol Methods.* 1981; 45: 65-78.
- Laborde E, Macsata RW, Meng F, Peterson BT, Robinson L, Schow SR, et al. Discovery, Optimization, and Pharmacological Characterization of Novel Heteroarylphenylureas Antagonists of C-C Chemokine Ligand 2 Function. *J Med Chem.* 2011; 54: 1667-81.
- Furuichi K, Wada T, Iwata Y, Kitagawa K, Kobayashi K-i, Hashimoto H, et al. CCR2 signaling contributes to ischemia-reperfusion injury in kidney. *J Am Soc Nephrol.* 2003; 14: 2503-15.
- Yang X, Gong H, Fu J, Quan G, Huang C, Luo Q. Molecular imaging of small animals with fluorescent proteins: From projection to multimodality. *Comput Med Imaging Graph.* 2012; 36: 259-63.
- ZHENG Y, HUANG C, CHENG Z, CHEN M. Establishment of Visible Animal Metastasis Models for Human Nasopharyngeal Carcinoma Based on a Far-Red Fluorescent Protein. *J Innov Opt Health Sci.* 2012; 5: 1250019.
- Zheng Y, Liu Y, Jin H, Pan S, Qian Y, Huang C, et al. Scavenger receptor B1 is a potential biomarker of human nasopharyngeal carcinoma and its growth is inhibited by HDL-mimetic nanoparticles. *Theranostics.* 2013; 3: 477-86.
- Ng LG, Hsu A, Mandell MA, Roediger B, Hoeller C, Mrass P, et al. Migratory dermal dendritic cells act as rapid sensors of protozoan parasites. *PLoS Pathog.* 2008; 4: e1000222.

29. Cahalan MD, Parker I. Choreography of cell motility and interaction dynamics imaged by two-photon microscopy in lymphoid organs. *Annu Rev Immunol.* 2008; 26: 585.
30. Miller MJ, Wei SH, Cahalan MD, Parker I. Autonomous T cell trafficking examined in vivo with intravital two-photon microscopy. *Proc Natl Acad Sci U S A.* 2003; 100: 2604-9.
31. Boissonnas A, Fetler L, Zeelenberg IS, Hugues S, Amigorena S. In vivo imaging of cytotoxic T cell infiltration and elimination of a solid tumor. *J Exp Med.* 2007; 204: 345-56.
32. Larson DR, Zipfel WR, Williams RM, Clark SW, Bruchez MP, Wise FW, et al. Water-soluble quantum dots for multiphoton fluorescence imaging in vivo. *Science.* 2003; 300: 1434-6.
33. Inoue H, Ando K, Wakisaka N, Matsuzaki K-i, Aihara M, Kumagai N. Effects of nitric oxide synthase inhibitors on vascular hyperpermeability with thermal injury in mice. *Nitric Oxide.* 2001; 5: 334-42.
34. Ding H, Wu F. Image Guided Biodistribution of Drugs and Drug Delivery. *Theranostics.* 2012; 2: 1037.
35. Nakasone ES, Askautrud HA, Kees T, Park J-H, Plaks V, Ewald AJ, et al. Imaging tumor-stroma interactions during chemotherapy reveals contributions of the microenvironment to resistance. *Cancer cell.* 2012; 21: 488-503.
36. Filipe-Santos O, Pescher P, Breart B, Lippuner C, Aebischer T, Glaichenhaus N, et al. A dynamic map of antigen recognition by CD4 T cells at the site of *Leishmania major* infection. *Cell Host Microbe.* 2009; 6: 23-33.
37. Yong K-T. Quantum dots for biophotonics. *Theranostics.* 2012; 2: 629.
38. Matheu MP, Beeton C, Garcia A, Chi V, Rangaraju S, Safrina O, et al. Imaging of effector memory T cells during a delayed-type hypersensitivity reaction and suppression by Kv1.3 channel block. *Immunity.* 2008; 29: 602-14.
39. Thomson AW, Turnquist HR, Raimondi G. Immunoregulatory functions of mTOR inhibition. *Nat Rev Immunol.* 2009; 9: 324-37.
40. Dumonde D. The role of the macrophage in delayed hypersensitivity. *Br Med Bull.* 1967; 23: 9-14.
41. Chen Y, Chen J, Liu Z, Liang S, Luan X, Long F, et al. Relationship between TH1/TH2 cytokines and immune tolerance in liver transplantation in rats. *Transplantation proceedings.* 2008; 40: 2691-5.
42. Theofilopoulos AN, Koundouris S, Kono DH, Lawson BR. The role of IFN-gamma in systemic lupus erythematosus: a challenge to the Th1/Th2 paradigm in autoimmunity. *Arthritis Res.* 2001; 3: 136-41.
43. Liu C, Gu Y. Noninvasive Optical Imaging of *Staphylococcus Aureus* Infection In Vivo Using an Antimicrobial Peptide Fragment Based Near-Infrared Fluorescent Probes. *J Innov Opt Health Sci.* 2013; 6: 1350026.
44. Sen D, Forrest L, Kepler TB, Parker I, Cahalan MD. Selective and site-specific mobilization of dermal dendritic cells and Langerhans cells by Th1-and Th2-polarizing adjuvants. *Proc Natl Acad Sci U S A.* 2010; 107: 8334-9.
45. Deane JA, Hickey MJ. Molecular mechanisms of leukocyte trafficking in T-cell-mediated skin inflammation: insights from intravital imaging. *Expert Rev Mol Med.* 2009; 11: e25.
46. Hwang JM, Yamanouchi J, Santamaria P, Kubes P. A critical temporal window for selectin-dependent CD4+ lymphocyte homing and initiation of late-phase inflammation in contact sensitivity. *J Exp Med.* 2004; 199: 1223-34.
47. Waite JC, Leiner I, Lauer P, Rae CS, Barbet G, Zheng H, et al. Dynamic imaging of the effector immune response to listeria infection in vivo. *PLoS Pathog.* 2011; 7: e1001326.
48. Molesworth-Kenyon S, Oakes J, Lausch R. A novel role for neutrophils as a source of T cell-recruiting chemokines IP-10 and Mig during the DTH response to HSV-1 antigen. *J Leukoc Biol.* 2005; 77: 552-9.
49. Kreisel D, Nava RG, Li W, Zinselmeyer BH, Wang B, Lai J, et al. In vivo two-photon imaging reveals monocyte-dependent neutrophil extravasation during pulmonary inflammation. *Proc Natl Acad Sci U S A.* 2010; 107: 18073-8.
50. Koedel U, Frankenberg T, Kirschnek S, Obermaier B, Häcker H, Paul R, et al. Apoptosis is essential for neutrophil functional shutdown and determines tissue damage in experimental pneumococcal meningitis. *PLoS Pathog.* 2009; 5: e1000461.
51. Ishida Y, Gao J-L, Murphy PM. Chemokine receptor CX<sub>3</sub>CR1 mediates skin wound healing by promoting macrophage and fibroblast accumulation and function. *J Immunol.* 2008; 180: 569-79.